Composite nanostructured growth of $(CdS)_{0.75}$ $(PbS)_{0.25}$/Si solar cell and its characterization

E. M. Nasir, I. S. Naji, A. A. Ramadhan
Department of Physics, College of Science, University of Baghdad, Baghdad, Iraq

By using vacuum evaporation, thin films of the $(CdS)_{0.75}$-$(PbS)_{0.25}$ alloy have been deposited to form a nanocrystalline composite. Investigations were made into the morphology, electrical, optical and I-V characteristics of $(CdS)_{0.75}$-$(PbS)_{0.25}$ films as-deposited and after annealing at various temperatures. According to AFM measurements, the values of grain sizes rise as annealing temperatures rise, showing that the films' crystallinity has been increased through heat treatment. In addition, heat treatment results in an increase in surface roughness values, suggesting rougher films that could be employed in more applications. The prepared films have direct energy band gaps, and these band gaps increase with the increase in the degrees of annealing temperature. Additionally, Urbach energy values decrease with an increase in annealing temperature degrees, indicating a reduction in the tail defects and an enhancement in crystal structure through annealing. The produced films' conductivity raise when temperature in the range (RT-473)K increased, demonstrating that they are semiconducting films. At comparatively lower temperature degrees, the conduction is caused by carriers that are stimulated into localized states at the band edges. At relatively higher temperatures, the conductivity appears to be substantially temperature-dependent. As a result, the conduction mechanism results from carriers being excited into extended states beyond mobility edges**.** The photovoltaic measurement (I–V) properties, open circuit voltage, short circuit current, efficiency and fill factor of $(CdS)_{0.75}$-$(PbS)_{0.25}$ heterostructure cells have been examined under 100mW/cm^2. Interestingly, rising annealing had enhanced photovoltaic cell performances; the solar cell had shown its highest efficiency (0.42%) at 573K. From XRD the structures are polycrystalline with cubic and hexagonal structures indicating that there's a mix of phases of PbS and CdS, the grain size and intensity raise with annealing temperatures.

(Received July 27, 2023; Accepted September 21, 2023)

Keywords: $(CdS)_{1-x}(PbS)_x$, AFM, Optical properties, Electrical properties

1. Introduction

The materials made of lead sulfide (PbS) and cadmium sulfide (CdS) have been selected to increase the conversion of solar energy from the ultra-violet to the NIR spectral region. Those II-VI group materials are suited for solar energy conversion and exhibit direct band gaps. Solar materials utilize PbS and CdS layers, respectively, as the absorber and window materials [1,2]. $Cd_{1-x}Pb_xS$ can be defined as one of the significant materials with a broad range of the applications in the selective coatings for effective photo-thermal conversion to get absorbance in UV-VIS area and reflectance in the infra-red region. This is because of the material's electrical, optical, and photoelectrical capabilities. Solar light could be controlledly absorbed and reflected using such films. Various practical applications, including infrared photo detectors, photoelectronics, solar cells, and optical switches, show promise for thin films of lead and cadmium sulfate [3]. CdS, one of the least expensive semiconducting materials from II-VI group, has received a lot of interest for its potential use in optoelectronic applications. As a result, the characterization and deposition of CdS semiconducting thin films had received much attention in the past few years. As a result of their advantageous optical characteristics, polycrystalline CdS thin films are frequently utilized as windows in a variety of heterojunction solar cells. It has been determined that cadmium sulfide films are a strong contender for the absorbing material in the

* Corresponding author: eman.nasir@sc.uobaghdad.edu.iq
https://doi.org/10.15251/JOR.2023.195.567

visible range [4, 5]. At room temperature, lead sulfide's energy band gap materials from 0.39 to 0.52 eV, but it can be altered by changing the bulk energy's form and size into nanocrystal structures. Lead sulfide is significant for infrared applications. As a result, the synthesis regarding PbS nanocrystals with various morphologies and the consequences on material properties are crucial in the quest for new uses for electroluminescent devices such LEDs. Because of its direct energy gap, lead sulfides are crucial for infrared applications. [6] CdS and PbS thin films have a broad range of the applications in the opto-electronics, chemistry (as gas, temperature, or catalysts or humidity sensors/), or solar control coatings, among other fields, thanks to their electrical, optical, and photoelectrical capabilities. [7]. In this research, the conditions for producing mixed $(CdS)_{0.75}$-$(PbS)_{0.25}$ thin films by vacuum evaporation over heated glass are established, and their properties as deposited films and after heat treatment are studied.

2. Experimental

Alloy was created utilizing materials of extreme purity. The Balzer Switzerland firm provided PbS and CdS with purity (99.999%), and the alloy was created with x=0.25 concentration. Carefully cleaning a quartz ampoule with water and alcohol, respectively, removed any grease, dust or other potential impurities. The appropriate amounts of PbS and CdS materials were weighed before being added to a quartz ampoule, which was after that sealed after being vacuumed to a pressure of 10^{-3} mbar. A furnace was used to gradually heat the sealed ampoule up to 1073K. After being kept at this temperature for roughly two hours, the ampoule was allowed to gradually drop to the temperature of the room. With the use of Edward (E306A) coating system and a vacuum of approximately (10^{-5}) mbar at a substrate temperature of 100°C, thin $(CdS)_{0.75}$–$(PbS)_{0.25}$ films were evaporated from the produced alloy. All films underwent heat treatments at (373, 473, 573) K. The optical, electrical and morphological characteristics of the thin $CdS)_{0.75}$-$(PbS)_{0.25}$ films with a (400nm) thickness have been examined using glass slides. Surface morphology measurements were made using an AFM (Scanning Probe Microscope type AA3000), which was provided by Angstrom Advanced Inc. With the use of a (UV-VISIBLE) spectrometer, measurements of the energy gap and optical calculations were made in the wavelength range of 190-1200 nm. Electrical measurements have been measured with D.C. conductivity. Kithely 2450 were used for I-V measurement, and XRD were measured by

3. Results and Discussions

When thin films of $(CdS)_{0.75}$-$(PbS)_{0.25}$ are deposited and annealed at (373, 573) K as shown in Figure 1, AFM is used for investigating the impact of annealing temperature on the surface morphology and grain size. All films have been found to be densely nanostructured, homogenous, and well-covered the substrate. The particles were all ordered uniformly, were all spherical in shape, and were evenly dispersed. When films are annealed at 573K and 373K, the values of grains sizes rise from 81.24nm for films that are deposited to 90.2nm and 86.20, respectively. The production of large grains may be caused by the aggregation of atoms on the surface at higher temperatures, which is consistent with another research [8,9]. This indicates that heat treatment has increased the films' crystallinity. The surface roughness degree is promoted by the heat treatment, according to AFM data. The surface roughness values regarding as-deposited and annealed films increase from (0.0537, 0.0564, 0.895) nm, suggesting an increase in the films' roughness, which could be employed in various applications. It indicates that during the initial stage of nucleation, particles (i.e. atoms) are adsorbed onto substrate to form the clusters. The clusters after that have a larger energy in comparison with the individual atoms, therefore at a higher annealing temperature, developing nuclei come in contact in order to form islands stage and appear to have a spherical shape. This is in keeping with previous literatures [10,11].

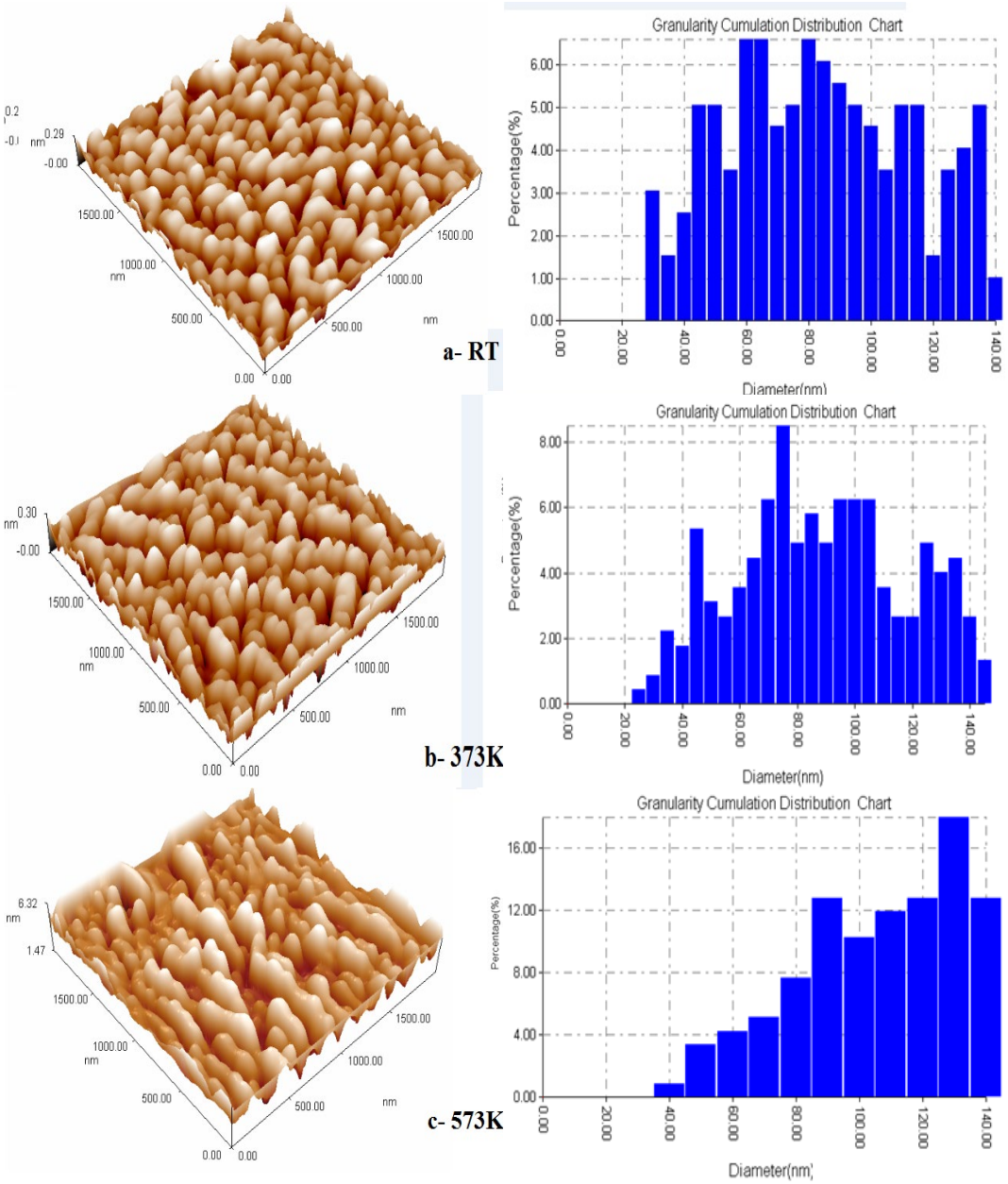

Fig. 1. AFM images of $(CdS)_{0.75}$-$(PbS)_{0.25}$ thin film at (a) (RT), (b) 373K, (c) 573K.

The optical characteristics of the deposited $(CdS)_{0.75}$-$(PbS)_{0.25}$ films on glass substrate were specified for both the deposited film and at various annealing temperatures (373, 473, and 573) K. The spectrum of absorption, transmittance has been determined as shown in Fig (2a, b). This figure demonstrates the great transparency of the films in visible range, as seen below at 500 nm the transmission varies between (47-72%) for (as deposited films-573K) and at 700 nm the transmission varies between (70-89%) for (as deposited films-573K). Additionally, as the annealing temperature rises, the transmittance rises as well, which implies the absorption decrease. Heating's impact on the transmission of $(CdS)_{0.75}$-$(PbS)_{0.25}$ films could be caused by a number of physical factors, including defect density, surface irregularity. Due to the produced films' crystallinity, it could be seen that there is a shift to a shorter wavelength as the annealing temperature is raised, followed by an increase in the energy gap value [10,11]. The superior crystal structure and surface features of films could be responsible for light scattering decrease, which

results in an increase in the degree of the transmittance. The current films' optical characteristics, crystal structure, and surface qualities are crucial for solar cell performance [10-13].

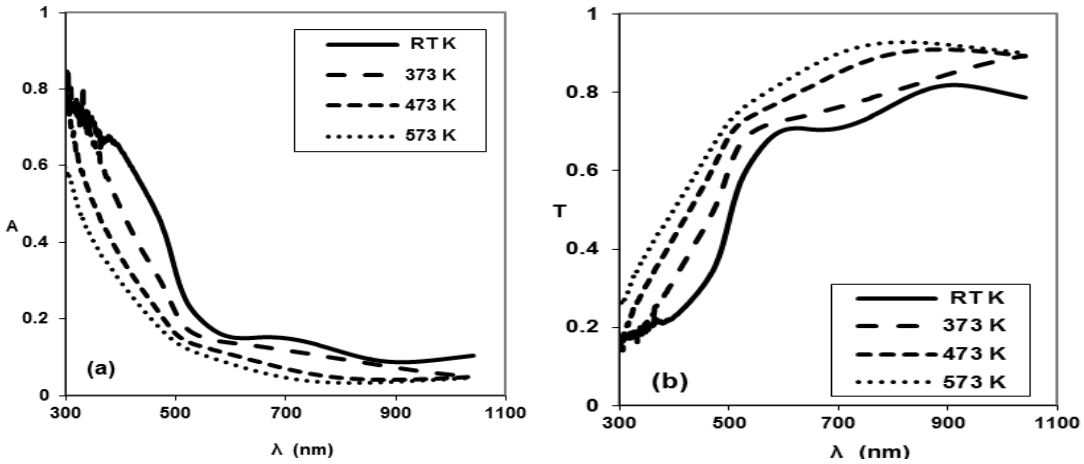

Fig. 2. The (a)-Transmittance and (b)- Absorptance spectra for $(CdS)_{0.75}$-$(PbS)_{0.25}$ thin films at various annealing temperatures.

Fig. (3a) illustrates how absorption coefficient of deposited $(CdS)_{0.75}$-$(PbS)_{0.25}$ films depend on the annealing temperature (T_a) as a function of wavelength. These data show that the $(CdS)_{0.75}$-$(PbS)_{0.25}$ films' absorption coefficient has been characterized by a high absorption at shorter wave-length region between 0.20 and 0.6 μm and by an absence of sharp edges on the long wavelength side from 0.64 to μ1.1 m. The coefficient of absorption shows high values at shorter wavelengths α ($\alpha > 10^4$), indicating a high likelihood of the permitted direct transition [10–12], and subsequently falls as wavelength increases. The absorption coefficient values are almost in agreement with the figures provided by [3,8,9]. The absorption coefficient (α) of $(CdS)_{0.75}$-$(PbS)_{0.25}$ films at various annealing temperatures (RT, 373, 473, 573K) is shown in Fig. 3a and may be computed using the following equation:

$$\alpha = 2.303\frac{A}{t} \tag{1}$$

where t and A represent the produced films' thickness and absorption, respectively [10–12]. Those figures show that at energies above the band gap, the absorption coefficient for the produced films attained greater values. This outcome is consistent with those of numerous other researchers [8–11]. According to Table 1, the absorption coefficient falls when annealing temperatures rise from (4.918 to 2.278) cm^{-1}, and this is because of the increasing energy gap with T_a. The degree of absorption loss during electromagnetic wave propagation through a medium is indicated by the extinction coefficient. Extinction coefficient (k) could be calculated from equation [10-12]:

$$k = \frac{\alpha\lambda}{4\pi} \tag{2}$$

Figure (3b) depict how the extinction coefficient of films made of $(CdS)_{0.75}$-$(PbS)_{0.25}$ behaves as annealing temperatures change. Those figures and Table (1) show that as the annealing temperature increases, the extinction coefficient falls. It is evident that for $(CdS)_{0.75}$-$(PbS)_{0.25}$ films as deposited, k reduces from 0.156 to 0.072 in the case where T^a increases from R.T. to 573 K because T_a increases diminish absorbance or the absorption coefficient, which causes k to decrease. [12]

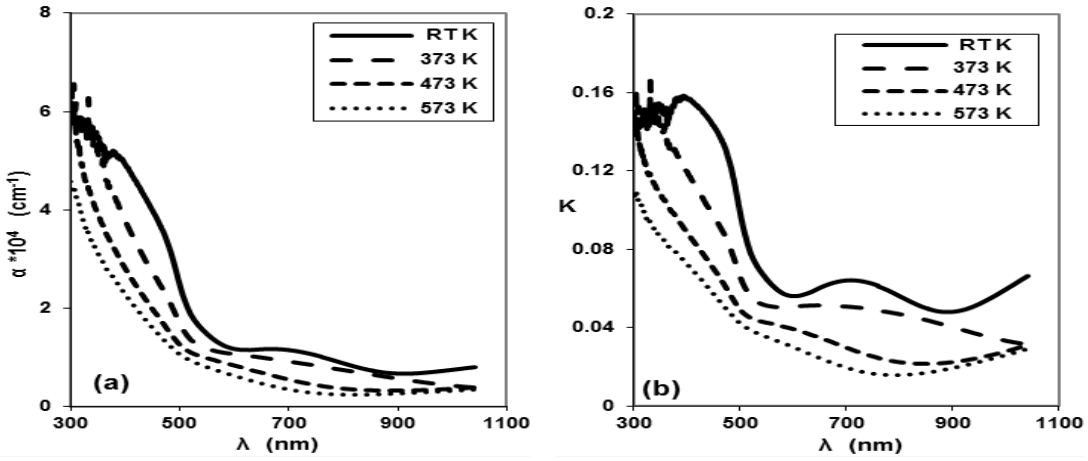

Fig. 3. The (a)- absorption coefficient and (b)- extinction coefficient spectra for $(CdS)_{0.75}$-$(PbS)_{0.25}$ films.

The optical energy gap values (E_g) for $(CdS)_{0.75}$-$(PbS)_{0.25}$ films were determined with the use of the Tauc equation that is utilized for finding the optical transition type [3,8-13]:

$$\alpha h\nu = B(h\nu - Eg)^r \tag{3}$$

a represents coefficient of absorption that is given by eq. (1), E_g represents the material's optical band gap, *B* represents a constant, *r* represents constant that equals (1/2) for the direct transition and *hv* optical band gap photon energy.

By plotting the relations of $(\alpha h\nu)^2$ vs. photon energy (hν) and choosing optimal linear part. It has been discovered that relation for r =(1/2) results in the linear dependence. A plot's linear nature is an indication of the fact that $(CdS)_{0.75}$-$(PbS)_{0.25}$ films have a direct band gap material. The extrapolation i.e. E_g, of portion at $[(\alpha h\nu)^2 = 0]$ has been shown in Fig.(4a). The value of the optical energy gap increases from 2.37eV to 2.94eV with the increase in annealing temperature degrees to 573K as can be seen from Table (1). The increasing of E_g with the increase of annealing temperatures is a result of the decrease of the defect states in band gap, meaning that heat treatment results in increasing the crystallite sizes and film structure enhancement. This is agreement with the result of AFM, and with results of researchers [11,13]. The absorption coefficient near fundamental absorption edge exponentially depends upon incident photon energy and is found by empirical Urbach tail relation that may be represented as follows [14-16]:

$$\alpha = \alpha_o \exp(h\upsilon / E_u) \tag{4}$$

where (α_o) represents a constant that is referred to as the band tailing parameter, E_u represents Urbach energy, indicating band tails of the localized states in the gap region and (hυ) represents incident photon energy, typically, E_u depends upon the temperature and describes localized state width and could be function of structural disorder [16]. From plots of Lnα as a photon energy function at different annealing temperature, Urbach energy has been estimated by taking reciprocals of linear portion slopes of those plots. It is observed that when E_g values increases the Urbach energy values decreases with increases annealing temperature as in Table(1). The decrease of E_u with increased annealing temperature could be a result of the decrease of defects in the tail states and to the improvement of crystal structure by annealing [3,7,8,10]

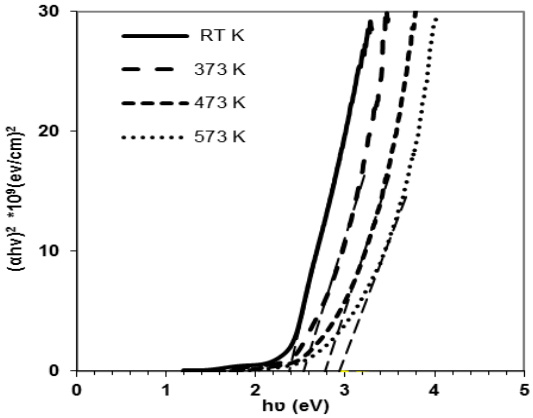

Fig. 4. $(\alpha h\upsilon)^2$ as a photon energy function for $(CdS)_{0.75}$-$(PbS)_{0.25}$ films at different annealing temperature (RT, 373,473,573)K.

In addition to that, the optical parameters of prepared films like the refractive index (*n*), coefficient of extinction (*k*), real ((ε_r) and imaginary ((ε_i) dielectric constant parts had been calculated from transmittance and absorbance spectra, which can be seen from Table 1. Those values have been higher in the composite $(CdS)_{0.75}$-$(PbS)_{0.25}$ films in comparison to individual CdS and PbS thin film values [8-13]. The refractive index for $(CdS)_{0.75}$-$(PbS)_{0.25}$ films was computed from eq.5 [14]:

$$n = \left(\frac{4R}{(R-1)^2} - k^2 \right)^{\frac{1}{2}} - \frac{(R+1)}{(R-1)} \tag{5}$$

where R represents reflectance and n is refractive index. Variation of refractive index as wavelength function is shown in Table.(1) . The refractive index is increased from (1.91-2.48) with increasing annealing temperatures from (RT-573)K.

The optical conductivity (σ_{op}) is one of the significant tools for studying electronic states in materials, it was calculated from the relation [15]:

$$\sigma_{op}=(\alpha nc/4\,\pi) \tag{6}$$

where (c) represents light velocity, Table (1) shows variations of the optical conductivity with T_a for $(CdS)_{0.75}$-$(PbS)_{0.25}$ thin films as deposited and after annealing. It is observed that these values decrease with increases of heat treatment because it depends upon absorption coefficient and refractive index. Real and imaginary dielectric constants have been determined by the use of eq.7 & eq. 8 [14-16]:

$$\varepsilon_r = n^2 - k^2 \tag{7}$$

$$\varepsilon_i = 2nk \tag{8}$$

The variation of real (ε_r) and imaginary (ε_i) dielectric constant parts for $(CdS)_{0.75}$-$(PbS)_{0.25}$ films with different annealing temperatures (RT to 573) K are shown in Table (1). The behavior of ε_r is the same as that of refractive index due to the smaller k^2 value in comparison to n^2 according to eq. (7) while ε_i is mainly dependent upon k values. It has been found that ε_r increase with the increase of the annealing temperatures. While ε_r decreases with the increase of annealing temperatures. In addition to that, ε_r found to increase from 3.62 to 6.18 for annealing temperatures between (RT to 573) K as listed in Table (1). And ε_i decreases from 0.59 to 0.36 for as deposited film and annealed films at 573K respectively.

Table 1. Optical properties of $(CdS)_{0.8}$-$(PbS)_{0.2}$ films at different annealing temperatures at λ=400nm.

T_a(K)	$\alpha *10^4$ (cm^{-1})	(K)	(n)	(ε_r)	(ε_i)	E_g (eV)	E_u(eV)	$\sigma_{op}(s^{-1})x10^{14}$
RT	4.918	0.156	1.91	3.62	0.59	2.37	1.023	2.24
373	3.763	0.119	2.38	5.67	0.57	2.53	0.981	2.14
473	2.786	0.088	2.53	6.43	0.45	2.76	0.609	1.69
573	2.278	0.072	2.48	6.18	0.36	2.94	0.4529	1.35

The variations of dark DC electrical conductivity (σ) with temperature (T) are shown in Fig. (5), the conductivity regarding all films increases with temperature in the range (RT-473) K, showing that the produced films are semiconducting, however the conductivity does not increase linearly with temperature [16, 17]. This could be explained by the structural alterations brought on by temperature on this film. In polycrystalline thin films, the structure (grain boundaries, grain size, structural flaws, etc.) has a significant rule on the electrical transport mechanism. As the film is being deposited, it has certain lattice imperfections in addition to physical and geometrical flaws that are dispersed randomly throughout the film's volume and surface. Grain boundaries and surface roughness are examples of geometric flaws in the volume. The structure plays a significant film in determining the physical characteristics of thin films. According to AFM studies, the structure regarding the film causes the average grain size to significantly increase as temperature rises, leading to a reduction in grain border area. This is the result of small crystallites coalescing into larger ones. The reduction in electron scattering brought on by such structural changes leads to the increase in the carrier concentration as the temperature rises. And as a result, the film's conductivity ultimately increases [16,18]. The activation energies E_{a2} and E_{a1} were estimated from slopes of curves in both regions with the use of equation, and the plots of (ln σ) vs 1000/T show two clearly distinct zones [16,17,18]

$$\sigma=\sigma_o \exp(E_a/KT) \tag{9}$$

where σ_o denotes pre-exponential factor, k represents Boltzmann's constant, E_a represents activation energy of electrical conduction, and T denotes absolute temperature. At a higher temperature (383K-473K), conductivity highly depends upon the temperature. Which is why, E_{a2} conduction mechanism in this case results from the carriers excited beyond edges of mobility into the extended states? At a rather lower temperature (RT-373K) conduction results from carriers that are excited into the localized states at the band edges [17].

The DC conductivity at RT (σ_{RT}), E_{a1} and E_{a2} values for $CdS)_{0.75}$-$(PbS)_{0.25}$ films at different annealing temperatures (RT, 373,473,573)K have been listed in Table (2), It is clear that the $\sigma_{R.T}$ decreases with the increase in the annealing temperature degrees, this is probably caused by the elimination of voids and the reduction of dangling bond concentration, which lead to a decrease in defect state, which results in an increase of energy gap and mobility. This is in agreement with the authors [16], similar behavior has been reported in the literature [17, 20]. Also, from Table (2), it is clear that the activation energies increase with the increase of the annealing temperature degrees due to the variation of the crystallinty of the film with increasing annealing temperature in terms of partial crystallization. These results are in agreement with [17-20].

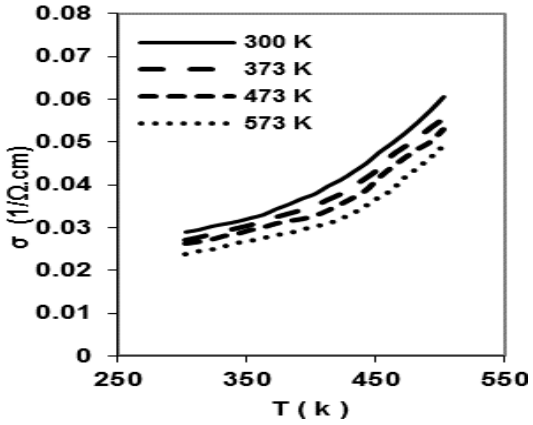

Fig. 5. Variation of (σ) with temperature as a function of $10^3/T$ for $(CdS)_{0.75}$-$(PbS)_{0.25}$ films at different annealing temperature (RT, 373,473,573)K.

Table 2. D.C. Conductivity parameters of$(CdS)_{0.75}$-$(PbS)_{0.25}$ films.

T_a(K)	σ_{RT} $(\Omega.cm)^{-1}$	Temp. range(K)	E_{a1}(eV)	Temp. range	E_{a2} (eV)
300	0.0289	303-413	0.132	423-503	0.0407
373	0.0271	303-413	0.146	423-503	0.0431
473	0.0263	303-413	0.163	423-503	0.0434
573	0.0238	303-413	0.217	423-503	0.0452

The i-v properties of $CdS)_{0.75}$-$(PbS)_{0.25}$ films have been evaluated at voltage of ($\pm$1V), with darkness and 25mW/cm^2 of light, at various annealing temperatures (RT, 373,473,573)K. The forward current appears to rise with voltage bias (V), and the dark current is noted to drop with annealing temperatures. This is due to the fact that heating improves crystal structure and results in a growth in crystallite grain size, causing the interface atoms to change arrangement, reducing dangling bonds, improving junction characteristics, and lowering dark current. I-V diagrams at different temperatures of annealing (RT, 373,473,573)K are shown in Fig. (6.) Using this equation, the ideality factor (***B***) is estimated. [21,22]

$$I = I_o\,(e^{qv/BKT} - 1) \tag{10}$$

where (I_o) is the saturation current, and I is the forward current in dark. The values of ideality factor *(B*) are calculated to be (7.15,6.9,5.4, 5.2) for (RT, 373,473,573)K respectively, Values of *(B*) reduce with rises in (T_a) due to improvements in the crystal structure caused by heating. The (I–V) plots of junction solar cells with light are given in Fig.(5). It is noticed that light current increases with rises in (T_a), and at RT, there doesn't appear to be any solar cell property, but it appears with the rise of annealing temperatures. The open-circuit voltage (Voc) of (0.55, 0.58,0.63)V and a short-circuit current (I_{sc}) is (0.122, 0.41, 0.34) mA for a (Ta) of (373,473,573)K respectively. The pen circuit voltage and short circuit current rise with increasing (T_a), due to an increase in energy band gap. The values of maximum voltage (V_m) and maximal current (I_m) have been inserted in Table (3).

.

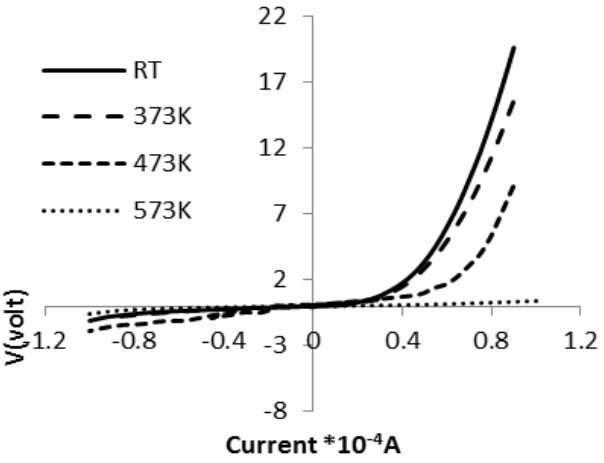

Fig. 5. I-V curve under dark for $(CdS)_{0.75}$-$(PbS)_{0.25}$/Si films at different annealing temperature (RT, 373,473,573)K.

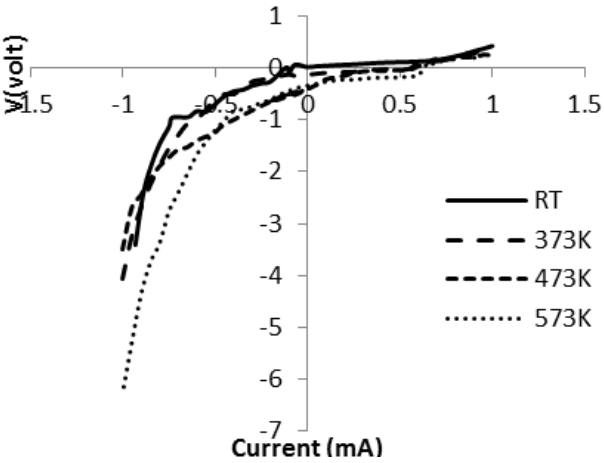

Fig. 6. I-V curve under light for $(CdS)_{0.75}$-$(PbS)_{0.25}$/Si films at different annealing temperature (RT, 373,473,573)K.

Table 3. Photovoltaic properties of$(CdS)_{0.75}$-$(PbS)_{0.25}$ /Si films.

T_a(K)	Im(mA)	Vm(V)	Pm(mwat)	Voc(V)	Isc mA	F.F	%η
373	0.069	0.234	0.016	0.55	0.122	0.240	0.072
473	0.145	0.199	0.029	0.58	0.41	0.122	0.129
573	0.499	0.186	0.093	0.63	0.34	0.433	0.412

The fill factor (F.F) and efficiency (η) are evaluated from the relations, [21,22]

$$F.F = \frac{Vm\ x\ Im}{Voc\ x\ Isc} \tag{9}$$

$$\eta = \frac{Voc\ x\ Isc\ x\ FF\ x\ 100}{Pin} \tag{10}$$

The P_{in} represents the input light intensity. The F.F and efficiency are found to vary between (0.24-0.433) and (0.072-0.412)% with a variation of (T_a) from (373-573)K respectively. In general, the efficiency is quite low, which could be attributed to factors such as photoelectrode resistivity and decreased absorption due to increased values of the energy gap. Also, the (η) increases with increasing annealing temperatures due to increased size of the grain, which can decrease particle-to-particle hopping of photo-induced carrier, and improve the crystal structure and reduce defects and imperfections, which can reduce recombination of the photo excited carriers, which result in high power conversion efficiency.XRD measurements of $(CdS)_{1-x}$ $(PbS)_x$ films at x content (0.25) are given in Fig.(1). From these figures, many diffraction peaks have appeared, which indicates that films are poly-crystalline in their nature with hexagonal and cubic structures, which indicates that there is a mix of the phases of PbS and CdS. The XRD pattern exhibits peaks corresponding to diffraction angles of 24.73°, 25.58°, 26.56°, 28.64°, and 30.92°, which are characteristics of the cubic phases (100), (111), (101). (200), and (220). In XRD pattern of the PbS film deposited, one characteristic peak of the CdS has been obtained, which is situated at the diffraction angle. In XRD pattern of the PbS film that had been deposited with the cadmium sulfate, only 1 peak that corresponds to the diffraction angles of 25.58° was obtained, which is a characteristic of cubic phase (111) [6]. In the XRD spectra, intensities of preferential orientation peak (111) along with other peaks have been higher. Thus, the film deposited shows much better crystalline behavior compared to the films that are deposited with the small annealing temperatures. Grain size (D) has been estimated with the use of the Scherrer formula [20]

$$D=K\lambda/\beta\cos\theta \tag{11}$$

where D represents grain size, k represents Scherrer constant (0.94), λ represents wave-length of X-ray utilized, β represents full width at half maximum (FWHM) and θ represents Bragg angle. Table1 shows crystallite size values and other micro-structural parameters. From this data, it's evident that Intensity and crystallite size increased significantly with the increment of annealing temperatures, where the relation between the crystallite size and the FWHM has been reversed. This is evidence of nanocrystal enhancement, which is an indication of the fact that, the deposited atoms of those films are going toward nano-structure. The strain (ε) has been calculated from the relations [3-6].

$$\varepsilon=\beta/4\tan\theta \tag{12}$$

The density of dislocation and the number of the crystallites per the unit surface area were determined with the use of the following formulas [21]

$$\delta=1/D^2 \tag{13}$$

$$N=t/D^3 \tag{14}$$

where δ represents dislocation density, N represents number of the crystallites per unit surface, and t represents thin film thickness, their values have been summarized in Table 4.

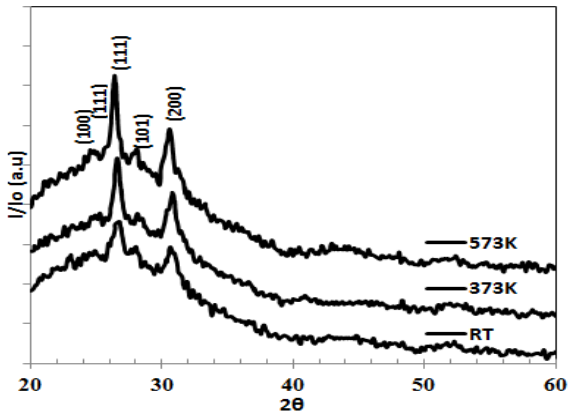

Fig. 7. XRD for $(CdS)_{0.75}$-$(PbS)_{0.25}$ films at different annealing temperature (RT, 373,573)K.

Table 4. The XRD parameters for the as deposited $(CdS)_{1-x}$-$(PbS)_x$ films and annealed at$(CdS)_{1-x}$ $(PbS)_x$.

X content	2θ (Deg.)	FWHM (Deg.)	d_{hkl} Exp.(Å)	G.S (nm)	Phase	I/Io	hkl	ξ $(1/\nu m^2)$* 10^{-3}	$\varepsilon*10^{-3}$
RT	24.73	0.2590	3.6330	31.4	CdS H	77	(100)	1.0142	5.155
	25.58	0.3290	3.5758	24.8	PbS C	79	(111)	1.6310	6.324
	26.56	0.3760	3.3533	21.7	CdS C	100	(101)	2.1219	6.951
	28.64	0.2820	3.1143	29.1	CdS H	72	(200)	1.1830	4.820
	30.92	0.3060	2.8896	26.9	CdS C	77	(220)	1.3782	4.828
373	24.58	0.2590	3.6330	31.4	CdS H	77	(100)	1.0147	5.187
	25.66	0.2590	3.5228	31.5	PbS C	80	(111)	1.0105	4.962
	26.58	0.4470	3.3508	18.3	CdS C	100	(101)	2.9987	8.257
	28.1	0.3060	3.1729	26.8	CdS H	74	(200)	1.3962	5.335
	30.97	0.4710	2.8970	17.5	CdS C	83	(220)	3.2645	7.418
573	24.58	0.259	3.6330	31.4	CdS H	77	(100)	1.0147	5.187
	25.66	0.259	3.4688	31.5	PbS C	82	(111)	1.0105	4.962
	26.4	0.474	3.3732	17.2	CdS C	100	(111)	3.3743	8.818
	28.1	0.306	3.1729	26.8	CdS H	78	(101)	1.3962	5.335
	30.95	0.565	2.9210	14.6	CdS C	85	(200)	4.6980	8.905

4. Conclusions

It is concluded that uniform, thin, adherent poly-crystalline $(CdS)_{0.75}$-$(PbS)_{0.25}$ thin films may be efficiently deposited through vacuum evaporation method at various annealing temperatures. Study was done on how annealing temperature affected optical, morphological, and electrical characteristics. According to AFM studies, heat treatment encourages an increase in grain size and degree of surface roughness. Because defect states are reducing as annealing temperatures rise, the energy gap values also raise which results in larger crystallites and improved structure. Because of an increase in energy gap, carrier density and particle size, electrical conductivity increases as temperature rises. The achieved qualities, such as morphology, optical properties and electrical properties, are crucial for the performance of the solar cells.

$(CdS)_{0.75}$-$(PbS)_{0.25}$ junction solar cells achieved efficiencies that ranged between 0.072% and 0.42% with increasing annealing temperatures. This enhancement can be a result of many reasons, mostly is crystalline quality of prepared thin films. Results further indicate that the annealing has an important effect on the solar efficiency.

References

[1] Mustafa K. A. Mohammed, Studying the Structural, Morphological, Plasmonics, volume 15, pages1989-1996(2020); https://doi.org/10.1007/s11468-020-01224-5

[2] Dulen Saikia, Pallabi Phukan, Thin Solid Films V.562(239-243)2014; https://doi.org/10.1016/j.tsf.2014.04.065

[3] Eman M. Nasir and Iqbal S. Naji, Australian Journal of Basic and Applied Sciences, 9(20) June 2015, Pages: 364-371.

[4] Ampong FK, Nkrumah I, Nkum RK, Boakye F., IJTRA. 2014; 2(6): 91-93.

[5] Rasha A. Abdullaha Faris S. Atallaha, Najat A. Dahhama, Mohammed. A.Razooqi, Eman M. Nasir, Nada M. Saeed, AIP Conf. Proc. 1476, 351-355 (2012); https://doi.org/10.1063/1.4751626

[6] Wang Y, Liu Z, Huo N, Huo N, Li F, Gu M, et al., Nat Commun. 2019; 10: 5136; https://doi.org/10.1038/s41467-019-13158-6

[7] V. Popescu, H. I. Naşcu, E. Darvasi, Journal of Optoelectronics and Advanced Materials **8**(3), 1187 (2006).

[8] Haneen S. Hakeem Nada K. Abbas, Baghdad Science Journal, 2021,18(3):640-648; https://doi.org/10.21123/bsj.2021.18.3.0640

[9] Hamid S. AL-Jumaili, Applied Physics Research; Vol. 4, No. 3; 2012, 75-82; https://doi.org/10.5539/apr.v4n3p75

[10] D. Qui˜nonez-Urias, A. Vera-Marquina,, D. Berman-Mendoza, et al, Optical Materials Express, Vol. 4, No. 11|, 2014; https://doi.org/10.1364/OME.4.002280

[11] A. Hasnat, J. Podder, Advances in Materials Physics and Chemistry, 2012, 2, 226-231; https://doi.org/10.4236/ampc.2012.24034

[12] Göde F, ünlü S., J. Nanoelectron. Optoelectron. 2019; 14(7): 939-944; https://doi.org/10.1166/jno.2019.2538

[13] Fatma Gode, Serdar Unlu, Materials Science in Semiconductor Processing 90 (2019) 92-100; https://doi.org/10.1016/j.mssp.2018.10.011

[14] J. I. Pankove, Optical Process in Semiconductors, Dover Publications, New York, (1971).

[15] S. H. Chaki, M.P. Deshpande, Jiten P. Tailor, Thin Solid Films 550 (2014) 291-297; https://doi.org/10.1016/j.tsf.2013.11.037

[16] J. S. Blakemore, Solid State Physics, 2nd ed., W. B. Saunders Company, Philadelphia, (1974).

[17] E. M. N. Al-Fwadi, M. F. Al-Alias & F. Y. M. Al-Shaikley, Iraqi Journal of Physics, Vol.5, No.1, 63-70(2008).

[18] Ikram Kamel abd Karem, Suhad A. Hamdan, Iraqi Journal of Science, 2022, Vol. 63, No. 6, pp: 2482-2491; https://doi.org/10.24996/ijs.2022.63.6.15

[19] T. Shekharam1, V. Laxminarasimha Rao, G. Yellaiah, T. Mohan Kumar and M. Nagabhushanam, Journal of Applied Physics, Volume 6, Issue 2 (2014), PP 34-39

[20] M. A. Barote, A. A. Yadav, L. P. Deshmukh, E. U. Masumdar, Journal of Non-Oxide Glasses Vol. 2, No 3, 2010, p. 151-165

[21] A. G. Milnes, D. L. Feucht, Heterojunctions and Metal Semiconductors Junctions, Academic Prees, London (1972); https://doi.org/10.1016/B978-0-12-498050-1.50007-6

[22] A. N. M. Ali, E. M. Nasir, Digest Journal of Nanomaterials and Biostructures,Vol.16, No.1, 2021, pp. 169 – 174.